RESULTS FROM THE DIII–D SCIENTIFIC RESEARCH PROGRAM

T.S. TAYLOR FOR THE DIII–D TEAM
DIII–D National Fusion Facility, General Atomics, San Diego, California 92186-5608

Abstract

The DIII–D research program is aimed at developing the scientific basis for advanced modes of operation which can enhance the commercial attractiveness of the tokamak as an energy producing system. Features that improve the attractiveness of the tokamak as a fusion power plant include: high power density (which demands high β), high ignition margin (high energy confinement time), and steady state operation with low recirculating power (high bootstrap fraction), as well as adequate divertor heat removal, particle and impurity control. This set of requirements emphasizes that the approach to improved performance must be an integrated approach, optimizing the plasma from the core, through the plasma edge and into the divertor. We have produced high performance ELMing H–mode plasmas with $\beta_N H_{98y} \sim 6$ for 5 τ_E (~1 s) and demonstrated that core transport barriers can be sustained for the length of the 5-s neutral beam pulse in L–mode plasmas. We have demonstrated off-axis electron cyclotron current drive for the first time in a tokamak, discovering an efficiency above theoretical expectations. Edge stability studies have shown that the H–mode edge pressure gradient is not limited by ballooning modes; the self-consistent bootstrap provides second stable regime access. Divertor experiments have provided a new understanding of convection and recombination in radiative divertors and have produced enhanced divertor radiation with scrape off layer plasma flows and impurity enrichment.

1. INTRODUCTION

The DIII–D research program is aimed at developing the scientific basis for advanced modes of operation which can enhance the commercial attractiveness of the tokamak as an energy producing system. Features that improve the attractiveness of the tokamak as a fusion power plant include: high power density (which demands high $\beta = 2\ \mu_o \langle P \rangle / B^2$), high ignition margin (high energy confinement time τ_E), and steady state operation with low recirculating power (high bootstrap fraction), as well as adequate divertor heat removal, particle and impurity control. This set of requirements emphasizes that the approach to improved performance must be an integrated approach, optimizing the plasma from the core, through the plasma edge and into the divertor. Research results from DIII–D reported here include results from all these areas.

In the area of core physics research, we have demonstrated improved plasma performance and increased duration of the high performance phase in both H–mode and L–mode plasmas. Moving towards an eventual goal of fully non-inductive current drive, we have made the first tokamak demonstration of off-axis electron cyclotron current drive. It exhibits higher off-axis efficiency than previously expected theoretically. In edge physics research, we have established the role of the self-consistently generated edge bootstrap current in stabilizing ballooning modes and allowing edge second regime access. Edge pressure gradients more than a factor of two above the ballooning limit without bootstrap current have been experimentally measured. This has improved our understanding of the edge pedestal and ELMs, which affect both core and divertor performance. In addition, a physics model of the density limit has been tested on DIII–D which reproduces density limit results on present machines and scales favorably to larger devices. In the area of heat and particle control in the divertor, we have established a new understanding of convection and recombination in radiative divertor plasmas. Finally, we have enhanced the divertor radiation by plasma flows and impurity enrichment.

2. PROGRESS TOWARDS INTEGRATED, STEADY-STATE, IMPROVED PERFORMANCE PLASMAS

In order to establish their future relevance for fusion, improved performance scenarios must demonstrate a path towards ultimate steady-state operation. This requires demonstrating that improved confinement plasmas can be sustained for long pulses at high beta values as well as developing the tools (e.g. current drive) which will be needed for steady state operation. DIII–D has carried out experiments in both these areas since the last IAEA.

Figure 1 demonstrates our recent progress in moving towards steady state improved performance discharges. In this figure, we measure our approach to steady state with $\tau_{duration}/\tau_E$, the duration of the high confinement phase divided by the energy confinement time. We measure advanced tokamak performance through the product of normalized beta, $\beta_N = \beta\ (aB_T/I_p)$, and the confinement enhancement factor H relative to the ITER confinement scaling law. For H–mode, we will use H_{98y}, which is defined relative to the most recent scaling for thermal energy confinement time in ELMing H–mode [1]. As can be seen in Fig. 1, significant progress has been made in DIII–D in the past two years in advancing both quantities. The points describing recent shots are above and to the right of our earlier results, which is the direction of our advanced tokamak goal.

An example of such an improved performance discharge is shown in Fig. 2 [2]. Lines indicating the β_N and H_{98y} values required for ITER and the ARIES-RS reactor study are also shown, indicating that this discharge exceeds the ARIES-RS requirements on the $\beta_N\ H_{98y}$ product. A $\beta_N\ H_{98y}$ product exceeding 6 is sustained for 1 s (5 τ_E). The high performance phase of the shot in Fig. 2 was terminated at about 3 s by the initiation of a neoclassical tearing mode, probably triggered by an ELM.

Two approaches have been taken to improve plasma performance and duration as is illustrated in Fig. 3. Both utilize the technique of an early neutral beam injection during the current ramp that was developed over the past several years in producing core transport barriers in DIII–D [3,4], JET [5], JT60-U [6],and TFTR [7,8]. However, one approach [2] is more aggressive in pushing high power to reach high β_N while the second has emphasized more the long pulse aspects. Neither shot shows the rapid, localized change in temperature gradient characteristic of a strong, localized core transport barrier; however, transport analysis indicates improvement in ion thermal diffusivity over most of the discharge relative to standard ELMing H–mode [2].

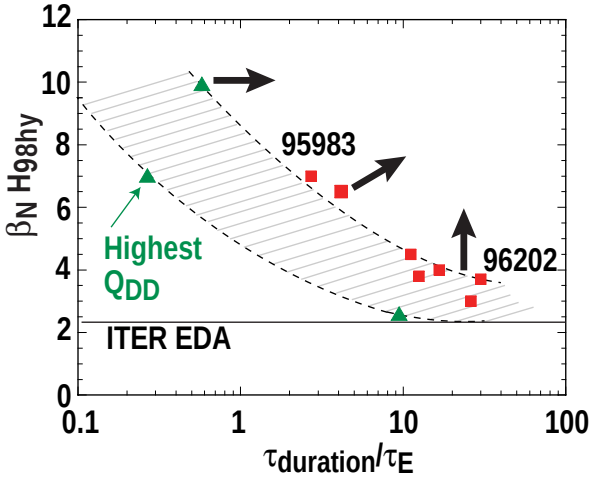

FIG. 1. Plot of the $\beta_N\ H$ product versus normalized discharge duration for DIII–D shots from the time of the 1996 IAEA meeting (triangles) and more recent shots (squares). The shaded region shows our progress. All these discharges are H–modes; accordingly, the confinement enhancement factor H_{98y} relative to the H–mode scaling is used.

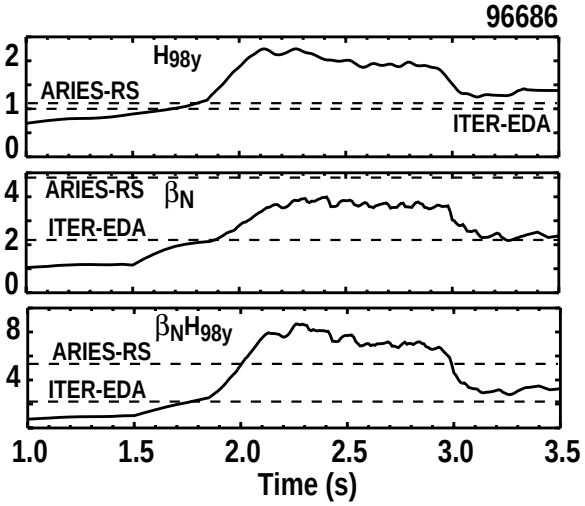

FIG. 2. Time evolution of a high performance DIII–D discharge. The 1 s duration is comparable to the current profile relaxation time scale. Some parameters of interest during the high performance phase are: $\beta \sim 4.5\%$, $n_e/n_{Gr} \sim 0.5$, $q(0) \sim 1, q_{95} = 4.4$, $\tau_{th} \sim .21$ s, and $f_{bs} \sim 50\%$, where n_{Gr} is the Greenwald density and f_{bs} is the bootstrap fraction.

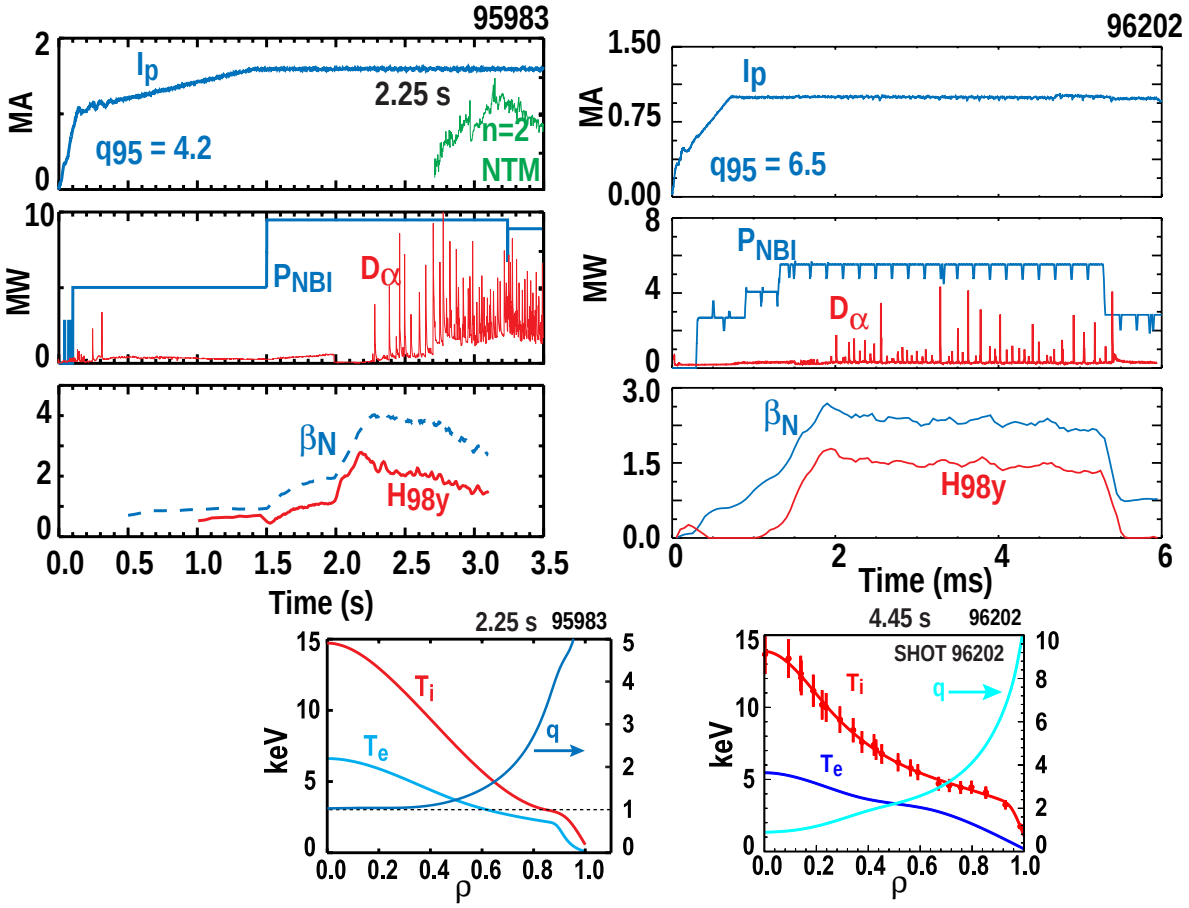

Fig. 3. Time histories and radial profiles of two recent DIII–D shots emphasizing long pulse high performance. Shot 95983 reached $\beta_N H_{98y}$ about 7 for 3 τ_E while 96202 achieved $\beta_N H_{98y}$ around 3 for 25 τ_E. (The corresponding β_N H products using the ITER89P L–mode scaling are 10 and 5. respectively.) The high performance phase of shot 96202 was terminated only when the neutral beam power was turned down while that of 95983 degraded due to the onset of neoclassical tearing modes. Shot 95983 was at 2.1 T toroidal field and had a line averaged density 5.4×10^{19} m^{-3} during the high performance phase while shot 96202 was at 1.9 T toroidal field and had a line averaged density of 2.7×10^{19} m^{-3}.

Core ion transport barriers have been run for even longer durations in low current, L–mode edge discharges, as is shown in Fig. 4. These shots were specifically optimized for the full 5 second neutral beam duration by running at low current and a relatively low density of 2×10^{19} m^{-3}. This discharge is an existence proof that it is possible to create an ion transport barrier which can last indefinitely.

A key feature in sustaining the good performance in the discharges in Figs. 3 and 4 is the absence of sawteeth. Detailed analysis of the current diffusion in these shots shows that this result is somewhat surprising, since neutral beam current drive alone should be enough to drive q(0) well below one. However, fast-particle driven MHD modes apparently broaden the neutral beam current drive profile, preventing this drop in q(0). In the discharges in Fig. 3, we observe fishbone oscillations while in the shot in Fig. 4, there are Alfvén eigenmodes present. Both of these modes are driven by fast particles and can redistribute these particles outward in radius.

Two major hurdles must be overcome in order to extend the discharges shown in Fig. 3 to higher performance and longer duration. First, as is shown in Fig. 3 (a), the performance in shot 95983 is degraded after 2.7 seconds by the onset of neoclassical tearing modes. This problem with neoclassical tearing modes is a common feature of many high performance discharges [2]. These modes are metastable, requiring a finite-size magnetic island to trigger instability. Finite-sized, seed islands can be triggered transiently, for example, by other MHD instabilities in the plasma, (e.g. sawteeth, ELMs

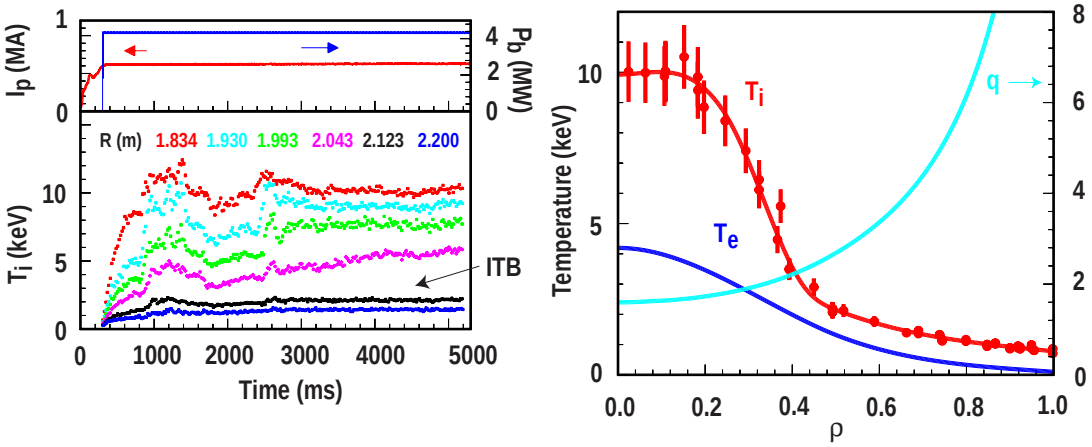

Fig. 4. Long pulse, L–mode edge discharge 94777 run at 1.9 T toroidal field. As is shown by the ion temperature time history, the core ion transport barrier lasts about 4.5 seconds in this shot, limited only by the duration of the neutral beam pulse. The major radius of the ion temperature measurements is listed at the top of the temperature figure. By the end of the beam pulse, even the q profile had essentially reached steady state, monotonic shape with q(0) = 1.6.

or fishbones). As is shown in Fig. 5, the absence of sawteeth in shots like those in Fig. 3 removes one of the possible sources of seed islands for the neoclassical tearing mode and thus allows operation at a higher beta value.

The second hurdle is overcoming the effects of current diffusion so that q(0) remains above one, preventing destruction of the core transport barriers by sawteeth and removing this trigger of neoclassical tearing modes. Although sawteeth were not present in the shots in Figs. 3 and 4, the MHD oscillations which we believe broadened the beam driven current are undesirable from a performance standpoint. The measured fusion neutron rate in the shot in Fig. 4, for example, was about 1/3 of the value predicted assuming all the fast ions deposited near the axis slowed down where they were born. As is discussed presently, the electron cyclotron heating (ECH) systems now coming on line on DIII–D should allow us to confront both these hurdles through electron cyclotron current drive to both broaden the current profile and shrink the seed island.

Because of the need for current profile control for advanced tokamak operation, investigation of electron cyclotron current drive (ECCD) is a key portion of the DIII–D research. In the past year, we have demonstrated off-axis ECCD on DIII–D for the first time in any tokamak [10]. Electron cyclotron wave power at 110 GHz, which is resonant near the second harmonic of the electron cyclotron resonance, can be steered over a range of minor radii by tilting the launching mirror in the poloidal direction. The waves are given a toroidal velocity component so they interact with electrons traveling in a preferred toroidal direction, generating toroidal current. Analysis was carried out using motional Stark effect measurements of the internal magnetic field, allowing the local driven current density to be determined [11]. A 4-point vertical scan of the deposition location was made, covering the range of 0.1 to 0.5 in normalized minor radius ρ. Figure 6(a) shows the profile of ECCD which is driven at a ρ = 0.5 by 1 MW of electron cyclotron power. The integrated net current driven is 35 kA. The gross behavior of the plasma--the evolution of the internal inductance, the time duration before the entry of the q=1 surface into the plasma as signified by the start of sawteeth — is consistent with the effects expected from the measured current drive for the different locations of the power deposition. The magnitude of the driven current exceeds the value calculated by linear (TORAY) or quasi-linear (CQL3D) codes. As is shown in Fig. 6(b), the theoretically predicted fall off in normalized efficiency with minor radius is not observed; the normalized efficiency at ρ = 0.1 and ρ = 0.5 are about the same. This result suggests that trapping of the heated electrons is much weaker than theoretically expected under the experimental conditions. These results strongly support the use of higher power ECCD as a means of sustaining current profiles with the optimized magnetic shear needed for advanced tokamak plasmas.

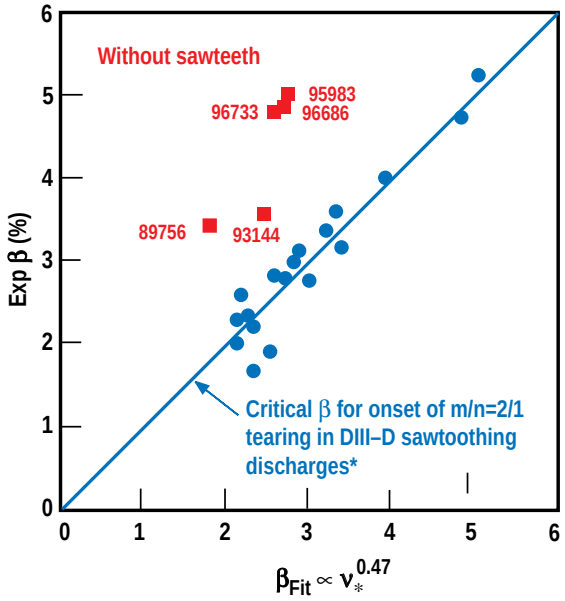

FIG. 5. The measured beta value for discharges similar to those in Fig. 2 (squares) significantly exceeds the neoclassical tearing mode limit established for sawtoothing discharges. The horizontal axis is the scaling value established in Ref. [9] while the line through the circular points is the best fit to the data for sawtoothing discharges. These neoclassical tearing modes are a mix of m/n = 3/2 and 2/1 cases.

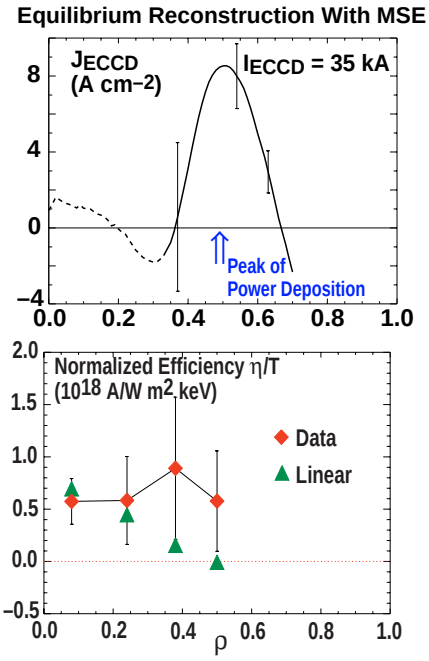

FIG. 6. (a) Profile of current density driven by ECCD for a case with power deposition at about half of the minor radius. (b) Normalized efficiency for ECCD as a function of the minor radius coordinate ρ. The current drive efficiency η has been normalized by the local electron temperature to remove the theoretically expected temperature dependence. The experimental results are compared to the linear TORAY calculations and show little decrease in normalized efficiency with ρ, contrary to theoretical expectations.

3. PROGRESS IN UNDERSTANDING AND CONTROLLING CORE TRANSPORT

In order to extend the improved performance results from present machines to future devices with confidence, we must finally develop a predictive understanding of tokamak transport. In addition, improved performance scenarios, especially in self-heated burning plasmas, will require development of new tools to control transport. Over the past two years, we have made progress in both understanding and control.

Over the past several years, fusion theorists have developed several new models of plasma transport [12-15]. Averaged over a large database of shots, each of these models do about equally well in predicting quasi-steady-state, equilibrium plasma profiles even though each model has a different mix of fundamental physics. Accordingly, to distinguish between models, some other test is needed.

Simulations have shown that perturbative transport experiments can provide a more critical test of transport models than equilibrium transport analysis. A perturbation source that deposits heat locally into the plasma particle species under study is preferred. Experiments have been performed on DIII–D using modulated ECH as the spatially localized perturbative heat source with the resonance absorption layer off axis. The electron and ion temperature responses are measured and the amplitude and phase of the perturbations (Fig. 7) and the equilibrium temperature profiles are compared to predictions from several transport models [16].

The results with off-axis heating indicate the electron and ion responses to the ECH perturbation are out of phase with each other at the plasma core and at the resonance layer. In general, the IFS-PPPL [12] and GLF23 [13] models predict reasonably well the ion response while the GLF23 and IIF [14] models do a reasonable job with the electron response. The GLF23 model includes the effects of

both electron temperature gradient (ETG) and ion temperature gradient (ITG) driven turbulence as well as trapped particle modes, which may be why it fits the best overall. The GLF23 model fits the data best for the case with the ECH localized at $\rho = 0.3$; the comparisons for other heating locations were somewhat worse [16]. None of the models showed good agreement with both the ion and electron perturbative responses and the equilibrium profiles although the equilibrium profile fit of the GLF23 model was improved by including the effects of the measured, average E×B shear [16].

Although the creation of ion thermal and angular momentum transport barriers has been connected with E×B shear stabilization of turbulence both theoretically and experimentally [17–19], the physics governing the electron channel is much less well understood. Electron thermal transport barriers are much more difficult to form in DIII–D than ion barriers and seem to require much greater magnetic shear [20]. Electron heating with either ECH or fast waves has been used to probe the physics of core transport barriers [21,22]. For reasons that are not completely clear, central electron heating during the end of the core ion barrier formation phase tends to weaken the ion barrier, resulting in some reduction in core ion temperature and core ion rotation. This effect occurs only within the core barrier region with the ion profiles outside this region remaining unchanged by the additional electron heating. Both ion and electron thermal diffusivities increase after the application of the electron heating, with the electron diffusivity rising almost an order of magnitude [21]. The changes in the ion channel in these discharges are consistent with change in the E×B shearing rate relative to the low k turbulence growth rates [21]. The decreased ion rotation gives a decreased E×B shear while the growth rate changes little. However, the physics of the electron channel in these plasmas remains unexplained [21]. New FIR scattering measurements of short wavelength turbulence at $k = 12\ cm^{-1}$ have shown measurable turbulence whose onset is correlated with the start of the electron heating, which suggests high k turbulence may be affecting electron transport. Detailed stability calculations, however, have not yet identified an associated unstable mode [21].

A connection between confinement improvement and observed and calculated turbulence reduction has also been established in discharges run with neon or argon injection to reproduce the TEXTOR RI-mode plasmas [23,24]. As is shown in Fig. 8, injection of neon results in dramatic reduction in density fluctuations observed by beam emission spectroscopy around $\rho = 0.8$. As the fluctuations gradually decrease, confinement improves. Furthermore, calculations of gyrokinetic stability similar to those done in [18,25] demonstrate that adding neon to the plasma reduces the linear growth rate at all wavenumbers, consistent with the observed confinement improvement. As indicated in Fig. 8, the turbulence at smaller wavenumbers should already be stabilized by E×B shear effects. Similar effects have been seen with argon injection. In these shots, transport analysis demonstrates an improvement in both electron and ion thermal transport which correlates with the reduction in observed density fluctuations. An important feature of these discharges, relevant to the edge stability issues discussed in the next section, is the reduction in edge pressure gradient and edge bootstrap current in H–mode plasmas with neon or argon impurity injection. In spite of the edge pressure pedestal reduction, energy confinement remains the same or improves in these plasmas.

4. EDGE PLASMA CONFINEMENT AND STABILITY

Another factor in obtaining steady-state improved performance discharges is control of edge transport and stability. The confinement physics and MHD stability of the H–mode edge pedestal affect both core plasma and divertor performance. The pedestal height influences overall plasma confinement, as is shown in Fig. 9. In addition, edge stability affects ELM frequency and amplitude, which have a major impact both on core transport barriers and on the divertor. Furthermore, impurity radiation in this edge region is a possible cause of the density limit. Finally, the interaction of the core plasma with the wall can have a major effect on the global MHD beta limits. Accordingly, understanding and controlling the physics of this edge region is a key issue for any future plasma which employs H–mode. In the past two years, DIII–D has demonstrated a strong connection between the pedestal height and core confinement and has demonstrated that the edge pressure gradients are not limited by the ballooning instability. In addition, we have shown that a model based on edge impurity radiation leads to a density limit very similar to the Greenwald prediction in present devices which scales much more favorably with machine size than previously anticipated. Finally, investigation of the physics of resistive wall modes has achieved β values up to 1.4 times the limit with no wall stabilization, has extended the duration of the wall stabilized period by a factor of three, and has produced a successful first attempt at active stabilization of the mode.

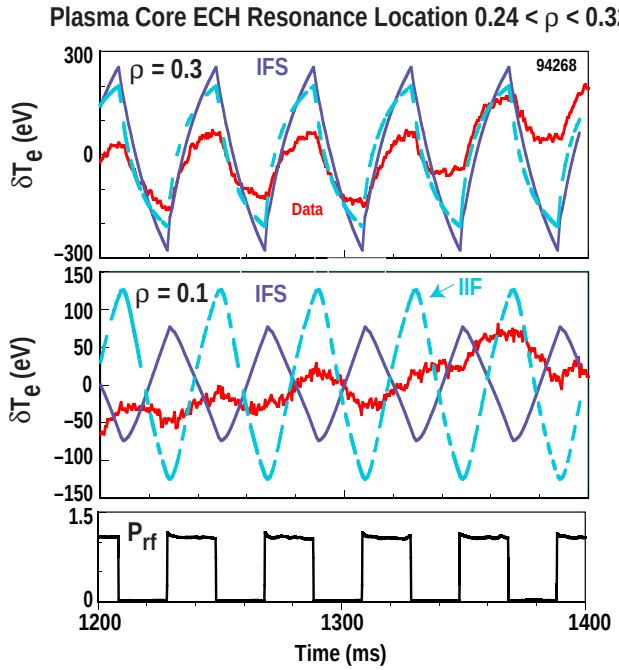

FIG. 7. Perturbed electron temperature, δT_e (eV), at $\rho = 0.3$ and $\rho = 0.1$ for measured data (solid, black lines), and simulated data from the IFS/PPPL model (solid gray lines) and IIF model (dashed gray lines). The ECH resonance location is at about $\rho = 0.3$.

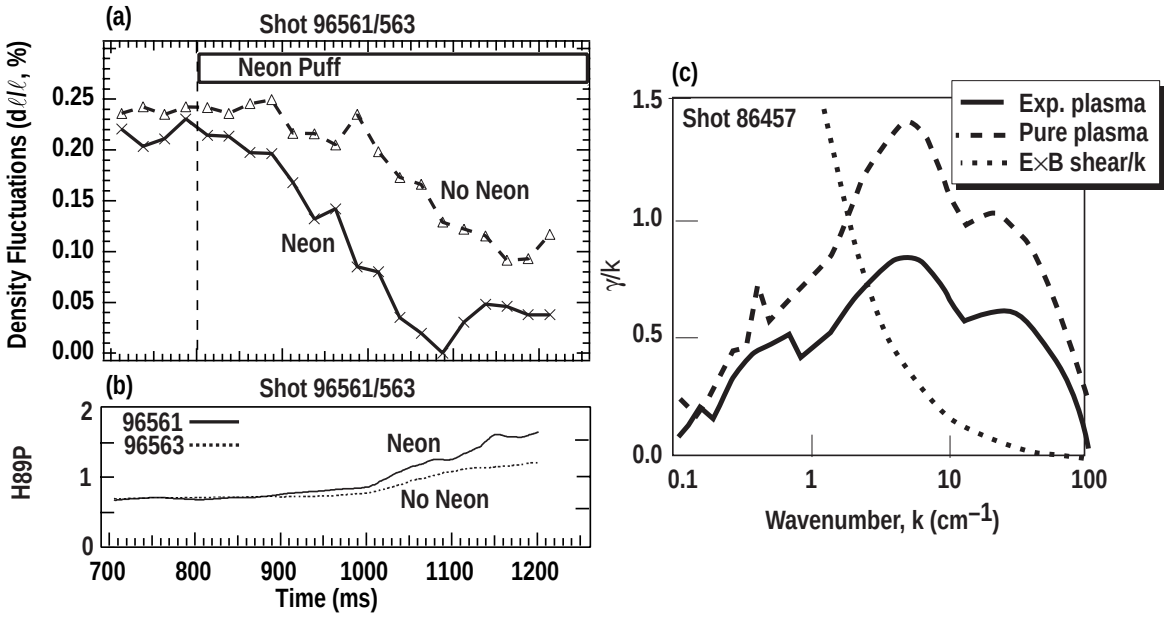

FIG. 8. Reductions in density fluctuations with neon impurity injection,(a), have been observed in L–mode discharges and may contribute to improved confinement,(b). For these L–mode discharges, the confinement enhancement factor is compared to ITER89P L–mode scaling. Gyro-kinetic stability code calculations for a similar discharge show that neon impurities in the mantle region, ρ~0.8, can reduce drift wave growth rates, (c), leading to stabilization of high k ETG modes. E×B shear is also large enough to affect the lower k turbulence associated with ITG modes.

Both theoretical expectations [26,27] and the DIII–D results shown in Fig. 9 [28] indicate a connection between the edge pressure pedestal height and the overall energy confinement. This connection is much deeper than the trivial one provided by the edge setting the boundary condition for the plasma core, since a boundary condition effect with no other influence would simply produce a linear relationship between the pedestal pressure and the total stored energy which is not seen experimentally. In the absence of any other constraint, one would naturally want to optimize plasma

performance by pushing the edge pedestal pressure to its maximum possible value to improve the energy confinement. Unfortunately, the pedestal pressure is limited by the onset of ELMs. In addition, optimizing plasma shape for the highest possible pressure pedestal usually results in large energy loss per ELM. As has been discussed in the ITER context [29], such large energy loss would be difficult to design for in a large device. Accordingly, control of the edge is needed to obtain the best possible core performance while not adversely affecting the divertor.

Because the ELM physics influences both core confinement and divertor performance, we have undertaken a systematic study of edge plasma stability. Although there has been considerable speculation that the edge pressure gradient just before an ELM is limited by high-n ballooning, detailed measurements on DIII–D have shown that the pressure gradient exceeds this limit by at least a factor of two [28]. As is shown in Fig. 10, we have determined that including the self-consistent edge bootstrap current in the ballooning stability calculation makes a major difference in the stability conclusions [30]. The bootstrap current, driven by the large edge pressure gradient, opens up a ballooning second stable region at the plasma edge. Accordingly, the edge pressure is not limited by high-n ballooning but rather by other, lower n MHD modes which are probably driven unstable by the large pressure and current gradients that ballooning stability allows [31].

The highest performance DIII–D VH–mode and negative central shear H–mode discharges are limited by MHD stability at the edge of the plasma; the peak performance is usually terminated in these discharges by low to medium n ideal instabilities at the edge having the characteristics of a large ELM but which normally result in a loss of the transport barrier [32,33]. Recent analysis has demonstrated that the interaction of low n ideal kink and high n ballooning stability plays a crucial role in the attainment and sustainment of high performance. High n ideal ballooning second stability access permits the buildup of the edge pressure gradient. This allows high peak performance but ultimately results in destabilization of the more dangerous low n global edge instabilities which are manifested as the large ELMs that terminate the high performance. Conversely, closing the second stable access at the edge generally limits the pressure gradient and bootstrap current to values well

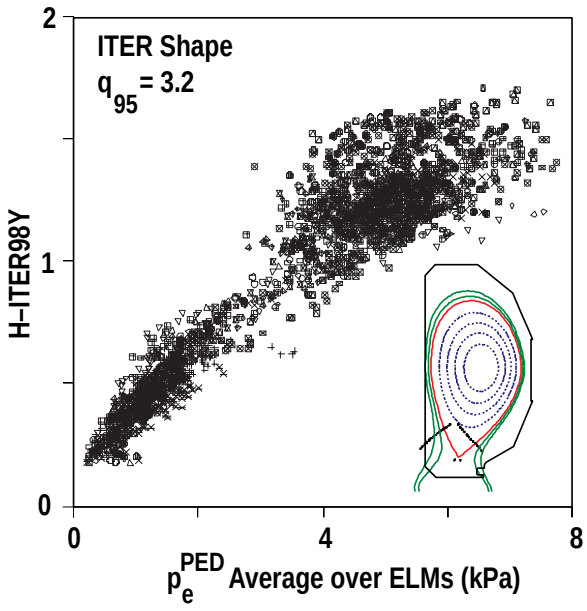

FIG. 9. H–mode energy confinement enhancement factor relative to ITER98 ELMy H–mode scaling increases with increasing H–mode pedestal pressure averaged over ELMs. The increase is approximately $P_{PED}^{2/3}$. This plot includes both Ohmic, L–mode and H–mode phases of a series of shots run in the ITER shape, which has a vertical elongation of 1.75, average triangularity of 0.24 and inverse aspect ratio of 0.34.

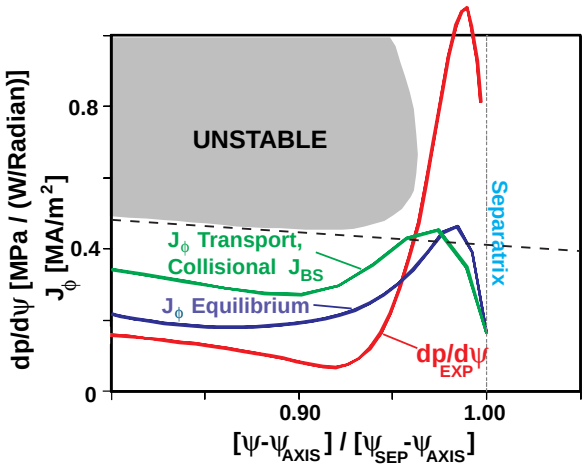

FIG. 10. Plot of the measured pressure gradient and inferred edge current density for a DIII–D discharge similar to those in Fig. 9: plasma current 1.5 MA, toroidal field 1.9 T, q_{95} = 3.4, inverse aspect ratio 0.36, vertical elongation 1.76, and average triangularity 0.28. The edge current density has been inferred from equilibrium reconstruction including MSE measurements and is compared with a transport calculation including a collisional bootstrap current model. The pressure gradients that would be unstable to high-n ballooning mode are shown. Note that the edge pressure gradient is not limited by ballooning modes and the experimental value greatly exceeds the ballooning limit that would be calculated by ignoring the bootstrap current, which is shown by the dashed line.

below the low and intermediate n kink limits. This results in lower peak performance with smaller amplitude ELMs which also allow longer discharge duration.

A clear route to long-pulse high-performance operation is, therefore, to control the edge conditions to eliminate second stable access, and to raise the first regime ballooning limit just below the low and intermediate n kink limits. One method for achieving this is through the cross section shape, which can be systematically varied using the DIII–D control system. Calculations have shown that the equilibrium squareness is a useful tool for controlling the edge ballooning stability through its effect on the field line connection length [31,34]. (As its name suggests, high positive squareness discharges have almost square shapes.) Large positive squareness, or low, or negative squareness, can restrict second stability access. This has been exploited in recent experiments in DIII–D [35] in which the ELM frequency is increased and the amplitude reduced at large squareness [31]. Motivated by these results, recent calculations show that higher order, local perturbations of the outboard shape, which greatly increase the field line connection length there, can also eliminate second stability access near the plasma edge, with little effect on the favorable low n kink stability properties of D-shaped plasmas [31]. This will be pursued in future experiments.

A second avenue for achieving control of the edge ballooning stability is to increase the edge collisionality to reduce the edge bootstrap current; lower edge current density hinders second stability access. Higher edge collisionality is achieved in DIII–D experiments by increasing the edge radiation by puffing deuterium and argon. In these experiments, the ELM frequency is typically reduced by roughly half and often the ELM magnitude is reduced as well. Figure 11 shows the time history of discharge 95011, in which argon was injected at 2 seconds. In this case, the ELM frequency was reduced by a factor greater than 2 with a small reduction in the ELM amplitude. The confinement is slightly improved by the change in ELM behavior. Figure 11(c) shows the calculated bootstrap current before and after the gas puff. The edge bootstrap current has been reduced and the peak is moved inward. This is reflected in the calculated ballooning stability in Fig. 11(b); the reduced edge bootstrap current has closed off the second stability access in this discharge.

A tokamak density limit scaling of the form $n_e \propto I_p/a^2$ has been reported by several authors [36,37] where I_p is the plasma current and a is the minor radius. However, extrapolation of this scaling to reactors can be misleading because the underlying physical processes have not been determined. We have conducted a series of experiments on DIII–D to determine the density-limiting processes in tokamaks [38,39]. Using the understanding gained through these experiments, we have succeeded in obtaining high confinement plasmas at densities well beyond the limit of the Hugill-Greenwald scaling [39,40]. A key result of these studies is that the n=0, m=1 MARFE condensation instability criterion [41] is in quantitative agreement with high resolution edge measurements on DIII–D [42]. Additionally, we have shown that the MARFE instability condition combined with ITER89P confinement scaling yields an edge density limit scaling of the form:

$$n_e^{crit} \propto \frac{I_p^{0.96}}{a^{1.9}} \xi^{-0.11} P_{heat}^{0.43} R^{0.17} B_T^{0.04} \left[\kappa^2(1+\kappa^2)\right]^{-0.22} \quad ,$$

where ξ_i is the impurity concentration and κ is the plasma elongation. Except for a moderate power dependence this scaling is remarkably similar to the Hugill-Greenwald scaling. The insensitivity to all plasma parameters except I_p and minor radius a derives from the fact that the MARFE density threshold for low Z impurities (e.g. oxygen or carbon) for an electron temperature range of 10–100 eV increases with the fourth power of T_e. Accordingly, a MARFE nearly always occurs at the same boundary temperature (~20 eV). Therefore, the trade off between density and temperature in the stored energy determines the density scaling. Thus, we conclude that future devices with high edge temperatures can access densities well above the nominal Hugill-Greenwald limit.

Turning now to the physics of wall stabilization, we have developed a double current ramp technique to reliably and reproducibly make plasmas where the β_N values achieved indicate that wall stabilization of MHD modes is important [43]. In addition, improved diagnostics have allowed us to make a direct identification of the resistive wall mode (RWM) mode structure in the plasma interior using ECE spectroscopy. Using these shots, we have achieved a new physics understanding of wall stabilization. We have produced rotating, wall stabilized discharges with the ratio of β_N to the no wall β_N limit E_w up to $E_w = 1.4 \pm 0.05$. For example, in shot 92544, E_w exceeds unity for 200 ms,which is

>30 τ_W. The time constant τ_W is the n =1 time constant of the wall (about 5.8 ms in this shot) and is a measure of the penetration time of the potentially unstable mode through the resistive vessel wall. Similar results with E_w well above unity have been obtained in a number of discharges run under similar conditions.

In all wall stabilized discharges, the plasma toroidal rotation is observed to slow down, which ultimately leads to destabilization of the resistive wall mode (RWM) when the plasma angular rotation speed Ω_{plasma} falls below some critical frequency Ω_c. The critical rotation speed Ω_c is robustly reproducible from shot to shot but is strongly dependent on plasma conditions, notably β_N. Investigation of the reasons for this decrease in Ω_{plasma} have determined a clear correlation between its onset and β_N exceeding $\beta_N^{no\,wall}$. However, there is no correlation of the slowing with fast particle driven MHD modes (TAE modes) or low n MHD activity during the slowing down period [44].

Active means of avoiding the RWM are being pursued by controlling either the plasma rotation or the RWM directly. As is shown in Fig. 12, preliminary results from open loop RWM control experiments have demonstrated that the RWM is suppressed by the application of an appropriate correction field using an external coil set located far outside the plasma. A series of discharges with reproducible RWM onset were run, but one discharge used an n = 1 (C-coil) perturbation which was

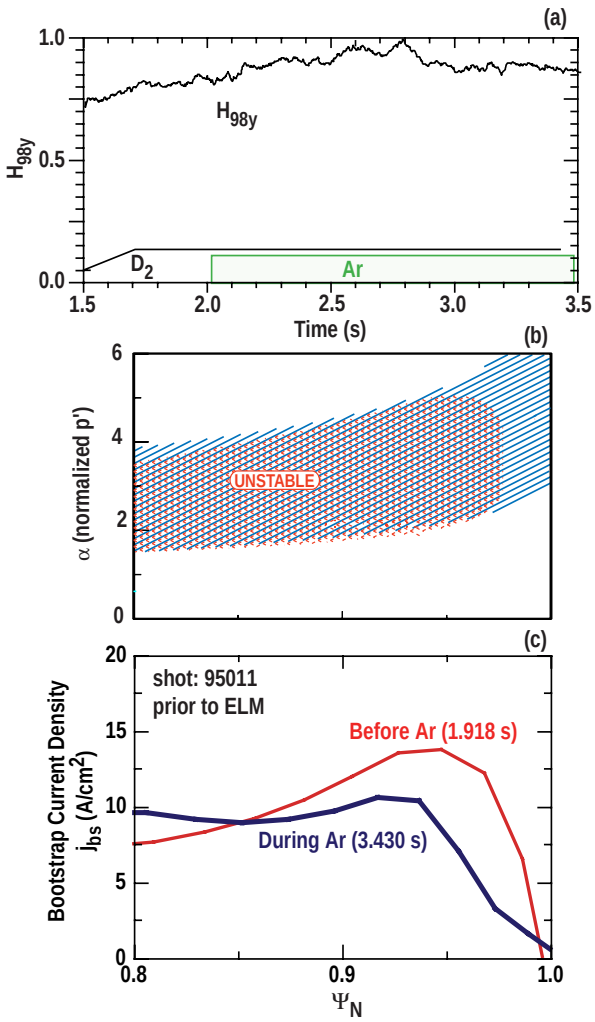

FIG. 11. Effect of Ar gas puffing on edge second stability access in discharge 95011. (a) Time history showing confinement enhancement H_{98Y} and D_2 and Ar injection (b) ballooning stability before and after injection of Ar and (c) computed bootstrap current density over the outer 20% of the plasma normalized flux.

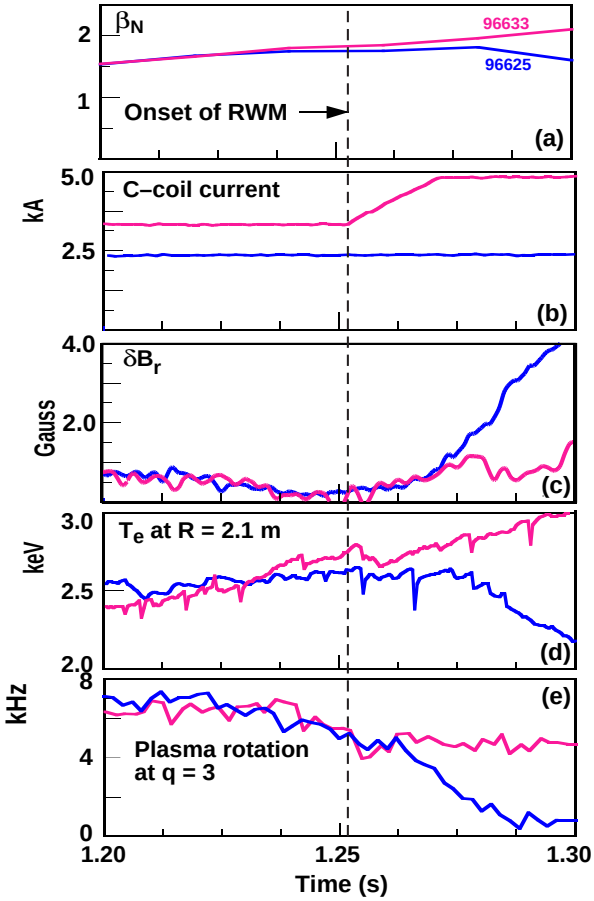

FIG. 12. Time history of discharges with (96633) and without (96625) pro-active control of the RWM (a) β_N (b) current in the C-coil (c) perturbed radial field measured on the saddle loops (d) ECE measurement of the electron temperature at R = 2.1 M. (e) plasma rotation at the q=3 surface. Note that the perturbed radial field grows without bound in the case with constant C-coil current but is stabilized by stepping up the C-coil current with the proper toroidal phase.

proactively programmed to turn on at the time of the RWM onset with a phase opposing the mode (Fig. 12). As observed from plasma rotation and T_e profiles near q = 3, the RWM started to grow but was suppressed and the plasma recovered when the opposing field was applied. The n=1 radial field soaking through the vacuum vessel wall was measured by a saddle loop array. As is shown in Fig. 12, this field grows without bound in the reference shot without the external n=1 field but remains at a low level with the external field applied, indicating that control was achieved. New experiments in DIII–D with new active feedback power supplies are planned next year to pursue this further.

5. DIVERTOR PHYSICS

The key issues in the divertor area are adequate heat removal and simultaneous control of particles and impurities. The major research focus has been on the radiative divertor with additional impurities to enhance the radiation. The challenge here is to maintain sufficient impurity density in the divertor to promote the needed radiation while simultaneously keeping the impurities from overwhelming the core plasma.

Through experiments on DIII–D[45-48] we have demonstrated the efficacy of using induced scrape-off-layer (SOL) flows to preferentially enrich impurities in the divertor plasma. These SOL flows are produced through simultaneous deuterium gas injection at the midplane and divertor exhaust using cryopumping. Using this SOL flow, an improvement in enrichment (defined as the ratio of impurity fraction in the divertor to that in the plasma core) has been observed for all impurities in trace-level experiments (i.e., impurity level is non-perturbative), with the degree of improvement increasing with impurity atomic number. In the case of argon, exhaust gas enrichment using a modest SOL flow is as high as 17. Using this induced SOL flow technique and argon injection, radiative plasmas have been produced that combine high radiation losses ($P_{rad}/P_{input} > 70\%$), low core fuel dilution ($Z_{eff} < 1.9$), and good core confinement ($\tau_E \gtrsim \tau_{E,ITER98Hy}$).

Besides the improvement in impurity enrichment, application of this technique causes several advantageous changes in the plasma [49]. First, at a high flow level, the SOL broadens and its density increases to 1.5×10^{19} m^{-3} while the electron temperature remains approximately 10 eV. Such profiles provide excellent screening of impurities emanating from the vessel wall and an excellent environment for impurity radiation. Second, the ELM amplitude is reduced by approximately a factor of two relative to standard ELMing H-mode conditions. This reduction is accompanied by a proportional increase in the ELM frequency such that the time-integrated energy carried out by the ELMs is approximately the same, but the instantaneous perturbation on the edge and divertor plasma induced by each ELM is much smaller. Modeling has also shown that the ELM dynamics are important in the obtainable impurity enrichment with higher frequency ELMs leading to improved enrichment. These changes are accomplished without significant impact on the core energy confinement.

At the previous IAEA, we reported that parallel thermal conduction based on measured divertor density and temperature profiles in detached plasmas is too small to account for the divertor heat flux and postulated that in the cold divertor zone the dominant transport process is convection along the field lines [38]. A one dimensional interpretive model of the detached divertor plasma [49] has been developed for further understanding of the experimental observations. The model calculates the parallel heat flux in the divertor plasma by integrating plasma radiation, obtained from an inversion of the bolometer data, from the target to a point in the divertor plasma and using the target heat flux, measured by an IR camera, as the boundary condition. The difference between this heat flux and the conduction heat flux, obtained from the measured T_e profile, yields the convective component of the heat flux. It is found that in attached plasmas, as shown in Fig. 13(a), the conduction component accounts for nearly all the heat flux. In contrast, in the detached case, the conduction channel is insignificant compared to the total heat flux [Fig. 13(b)] and convection at approximately the sound speed is required to account for most of the heat flux [Fig. 13(c)]. Furthermore, it is concluded that the observed intense radiation near the target plate must be due to volume recombination since the electron temperature measured by Thomson scattering is too low for excitation radiation.

These experimental results are supported by UEDGE modeling [50] which shows a broad regions of Mach ~ 0.4 and copious volume recombination near the target plate in detached plasmas [Fig. 14(a)]. Recent measurements confirm these experimental interpretations and UEDGE results. Visible and UV line ratio measurements [51,52] show direct evidence of volume recombination [Fig. 14(b)]. Plasma parallel flow speeds at or near the sound speed are also observed by spectroscopy [Fig. 14(c)] [51] as well as a Mach probe [53]. From Langmuir probe potential measurement [53], we

also deduce poloidal $E_r \times B_T$ flows. The flow direction depends on the direction of the toroidal field and heat and particle flux associated with it is estimated to contribute significantly to particle exchange between the two divertor strike points and could explain the field-dependent divertor in-out asymmetry.

We have recently installed a divertor baffle and cryopump [54] at the upper divertor whose shape is matched for particle control in high triangularity plasmas ($\delta \sim 0.7$). This installation, combined with the more open pumped lower divertor allows a direct comparison of the effects of geometry on divertor and core plasma performance. A comparison of open/closed divertor operation was carried out with carefully matched plasmas. The cryopumps in each divertor were turned off for this comparison. We observed that the line-average density was very similar in the two cases, but the midplane D_α was reduced in the closed divertor. The density profile was less steep near the separatrix for the closed case, and the temperature responded to keep the electron pressure roughly constant. Transport modeling [54] indicates that the core ionization source was reduced by a factor of about 2.6 in the closed case. No changes in energy confinement during ELMing H–mode operation were observed, but the line average density at which partial detachment occurred was decreased by 20% for the closed case. With the upper cryopump turned on, we achieved active density control with $n_e/n_{Gr} = 0.27$, which is similar to the 0.22 achieved with the lower pump. This establishes an important particle control tool for high triangularity plasma operation in DIII–D. In 1999, we will install a third divertor cryopump for the purpose of pumping the inner strike point in the upper divertor [54] . In addition, a structure in the private flux region which protects the inner pump will serve also as a baffle to reduce the recycling by an additional factor of 2 and isolate the two strike points.

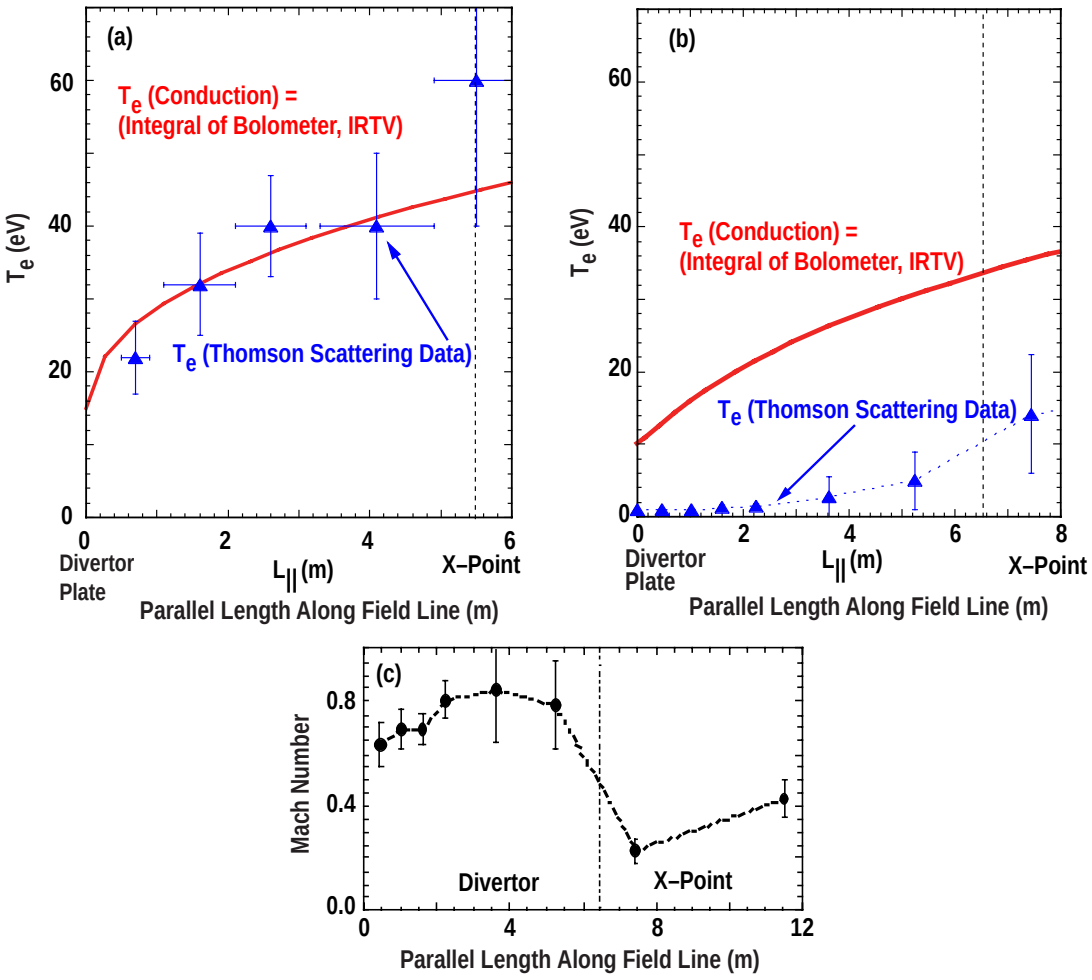

FIG. 13. (a) In attached plasmas, classical parallel conduction accounts for nearly all the divertor heat flux. (b) In the partially detached state the conduction channel is insignificant compared to the total heat flux. (c) Parallel flow Mach number near 1 can account for the balance of the heat flux.

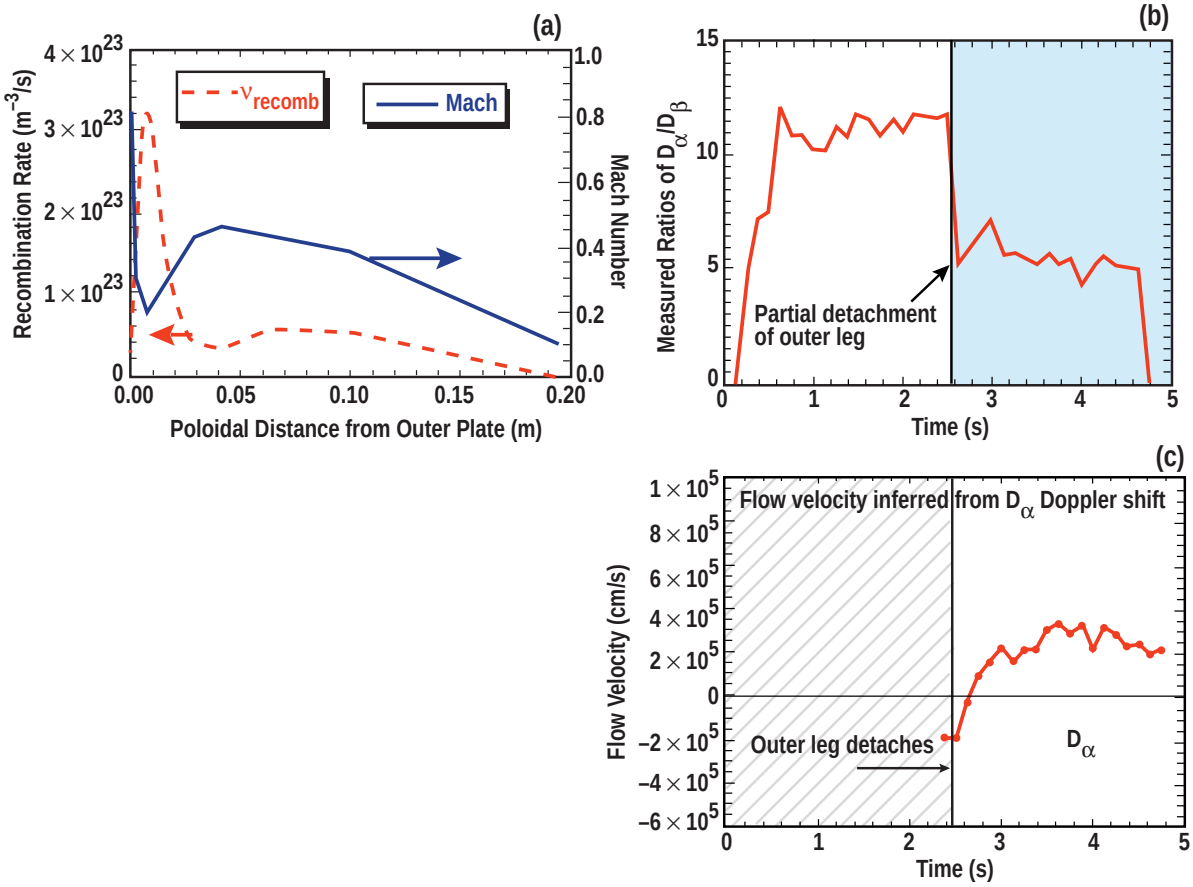

FIG. 14. (a) Modelling of a partially detached plasma shows Mach 0.4 flow in the bulk of the divertor plasma and copious volume recombination near the target plate. (b) D_α/D_β line ratio indicate recombination after detachment. (c) Flow speed of the order of 1/4 sound speed is measured by spectroscopy.

6. CONCLUSION

Research on DIII–D over the two years since the last IAEA meeting has made significant progress in the core, edge and divertor areas. We have demonstrated integrated, high performance ELMing H–mode plasmas with β_N H_{98y} ~ 6 for 5 τ_E (~1 s).

In the core physics area, we have

- Shown that core transport barriers can be sustained for the length of the neutral beam pulse (5 s) with no sign of degradation.
- Demonstrated off-axis electron cyclotron current drive with an efficiency well above theoretical expectations.
- Made critical tests of physics-based transport models.
- Produced evidence for passive and active wall stabilization of MHD modes.

In the edge physics area, we have

- Demonstrated the role of edge bootstrap current in edge second stability regime access.
- Developed and tested a physics model of the density limit which agrees with Hugill-Greenwald limit and which scales quite favorably to larger, hotter machines.

In the divertor physics area, we have

- Achieved a new understanding of convection and recombination in radiative divertor plasmas.
- Produced enhanced divertor radiation with scrape off layer plasma flows and impurity enrichment.

This scientific progress sets the stage for future DIII–D research. On a three year time scale, with 6 MW of ECH power, we are aiming at an integrated demonstration of advanced tokamak operation sustained for five seconds. In the nearer term, our experiments will emphasize expanding the spatial extent of internal transport barriers, regulating edge bootstrap currents, stabilizing neoclassical tearing modes, feedback stabilizing high-beta resistive wall modes, and developing the basis for radiative divertors in both single and double null configurations.

ACKNOWLEDGMENTS

This is a report of work supported by the U.S. Department of Energy under Contract Nos. DE-AC03-89ER51114, DE-AC05-96OR22464, DE-AC02-76CH03073, W-7405-ENG-48, and Grant No. DE-FG03-96ER54373.

The author would like to acknowledge the many contributions from the entire DIII–D Team in the research presented here. The contributions of Dr. D.R. Baker, G.L. Jackson, R.J. La Haye, M.A. Mahdavi, M. Murakami, R. Prater, T.C. Simonen, and A.D. Turnbull are specifically noted. The author would like to especially thank Dr. K.H. Burrell for assistance in this work and in the preparation of this manuscript.

REFERENCES

[1] ITER Physics Basis Document, Nuclear Fusion (to be published). JET report JET-P(98)-17.
[2] RICE, B.W., et al., these Proceedings.
[3] STRAIT, E.J. et al., Phys. Rev. Lett. **75**, 4421 (1995).
[4] RICE, B.W., Phys. Plasmas **3**, 1983 (1996).
[5] SÖLDNER, F.X., et al., Plasma Phys. Control. Fusion **39**, B353 (1997).
[6] KOIDE, Y., et al., Phys. Plasmas **4**, 1623 (1997).
[7] LEVINTON, F.M., et al., Phys. Rev. Lett **75**, 4417 (1995).
[8] SYNAKOWSKI, E.J., et al., Phys. Plasmas **4**, (1997).
[9] LA HAYE, R.J., et al.,, Plasma Phys. and Contr. Nucl. Fusion Research 1996 (IAEA, Vienna, 1997), Vol. 1, p. 747.
[10] LUCE, T.C., et al., these Proceedings.
[11] FOREST, C.B., et al., Phys. Rev. Lett **73**, 2244 (1994).
[12] KOTSCHENREUTHER, M., et al., Phys. Plasmas **2**, 2381 (1995).
[13] WALTZ, R.E., et al., Phys. Plasmas **4**, 2482 (1997).
[14] ITOH, S.I., et al., Phys. Rev. Lett. **72**, 1200 (1994).
[15] KINSEY, J.E., et al., Phys. Plasmas **3**, 3344 (1996).
[16] DEBOO, J.C., et al., these Proceedings.
[17] BURRELL, K.H., Phys. Plasmas **4**, 1499 (1997).
[18] STAEBLER, G.M. , et al., these Proceedings.
[19] SYNAKOWSKI, E.J., et al., these Proceedings.
[20] BURRELL, K.H., et al., Plasma Phys. Control. Fusion **40**, 1585 (1998).
[21] GREENFIELD, C.M., et al., these Proceedings.
[22] RETTIG, C.L., et al., Phys. Plasmas **5**, 1727 (1998).
[23] MESSIAEN, A.M., et al., Phys. Plasmas **4**,1690 (1997)..
[24] JACKSON, G.L., et al., Proc. of the 13th Int. Conf. on Plasma Surface Interactions, San Diego, California, 1998, to be published.
[25] STAEBLER, G.M. , et al, "Improved High Mode with Neon Injection in the DIII–D Tokamak," submitted to Phys. Rev. Lett.
[26] KOTSCHENREUTER, M., et al., Plasma Phys. and Contr. Nucl. Fusion Research 1996 (IAEA, Vienna, 1997) Vol. 2, p. 371.

[27] WALTZ, R.E., et al., Plasma Phys. and Contr. Nucl. Fusion Research 1996 (IAEA, Vienna, 1997) Vol 2, p. 385.
[28] OSBORNE, T.H., et al., Proc. of the 13th Intl Conf. on Plasma Surface Interactions, San Diego, California, 1998, to be published.
[29] LEONARD, A.W., et al., Proc. of the 13th Int. Conf. on Plasma Surface Interactions, San Diego, California, 1998, to be published.
[30] GRANETZ, R., OSBORNE, T.H., et al., these Proceedings.
[31] LAO, L.L., et al.,these Proceedings.
[32] STRAIT, E.J., et al., Contr. Fusion and Plasma Physics (Proc. 20th Euro. Conf. on Contr. Fusion and Plasma Physics, Lisbon 1993) (European Physical Society, Petit Lancy, 1994) Vol. 1, p. 211.
[33] STRAIT, E.J. , et al., Phys. Plasmas **4**, 1783, (1997).
[34] TURNBULL, A.D., et al., "Improved MHD Stability Through Optimization of Higher Order Moments in Cross Section Shape of Tokamaks," General Atomics Report GA-A22943 (1998), submitted to Phys. Plasmas.
[35] FERRON, J.R., et al., "Modification of Tokamak Edge Instability Character Through Control of Ballooning Mode Second Stability Regime Accessibility," submitted to Nucl. Fusion.
[36] HUGILL, J., et al., Heating in Toroidal Plasmas (Proc. 2nd Joint Varenna-Grenoble Int. Symp., Como, 1980), Vol. 2, CEC, Brussels (1980) 775.
[37] GREENWALD, M., et. al., Nucl. Fusion 2, 2199 (1988).
[38] MAHDAVI, M.A., et al., Plasma Phys. and Contr. Nucl.Fusion Research 1996 (IAEA, Vienna, 1997), Vol 1, p. 397.
[39] MAINGI, R., et al., these Proceedings.
[40] MAINGI, R.,et al., Phys. Plasmas **4**, 1752 (1997).
[41] DRAKE, J.F., Phys. Fluids **30**, 8 (1987).
[42] MAHDAVI, M.A., et al., Contr. Fusion and Plasma Phys. (Proc. 24th Euro. Conf. on Contr. Fusion and Plasma Physics, Berchtesgaden, 1997) (EPS Petit Lancy, 1997) Vol. 3, P. 1113.
[43] GAROFALO, A., et al., "A Study of Resistive Wall Modes in D III–D," in Contr. Fusion and Plasma Phys. (European Physical Society, Prague, 1998) to be published.
[44] GAROFALO, A.,et al., "Direct Observation of the Resistive Wall Mode in a Tokamak and Its Interaction With Plasma Rotation," General Atomics Report GA-A 22985 (1998), submitted to Phys. Rev. Lett.
[45] SCHAFFER, M.J., et al., Nucl. Fusion **8**, 1000 (1995).
[46] SCHAFFER, M.J. , et al., J. Nucl Mater. **241-243**, 585 (1997).
[47] WADE, M.R., et al., "Impurity Enrichment Studies with Induced Scrape-Off Layer Flow," Nucl. Fusion (accepted for publication) (1998).
[48] WADE, M.R., et al., "Impurity Entrainment Studies Using Induced SOL Flow in DIII–D," Proc. of the 13th Inter. Conf. on Plasma Surface Interactions in Contr. Fusion Devices, San Diego, California, 1998, to be published.
[49] LEONARD, A.W., et al., Phys. Rev. Lett. **78**, 4769 (1997).
[50] PORTER, G.D., et al., Phys. Plasmas **3**, 1967 (1997).
[51] ISLER, R.C., et al., Proc. of the 13th Inter. Conf. on Plasma Surface Interactions in Contr. Fusion Devices, San Diego, California, 1998, to be published .
[52] FENSTERMACHER, M.E., et al., "Physics of the Detached Radiative Divertor Regime in DIII–D," Proc. of the 25th EPS Conf. on Contr. Fusion and Plasma Phys., Prague, Czech Republic, 1998, to be published.
[53] BOEDO, J., et al., "Plasma Flow in the DIII–D Divertor," Proc. of the 25th EPS Conf. on Contr. Fusion and Plasma Phys., Prague, Czech Republic, 1998, to be published.
[54] ALLEN, S.L., et al., "Studies of Baffled and Open Pumped Divertor Operation on DIII–D," Proc. of the 13th Inter. Conf. on Plasma Surface Interactions in Contr. Fusion Devices, San Diego, California, 1998, to be published.

DIII–D TEAM

S.L. Allen,[a] P.M. Anderson,[b] M.E. Austin,[c] D.S. Baggest,[b] W. Baity,[d] D.R. Baker,[b] D.E. Baldwin,[b] G. Barber,[d] R. Bastasz,[e] C.B. Baxi,[b] L. Baylor,[d] S. Bernabei,[f] J. Bialek,[g] J.A. Boedo,[h] A. Bondeson,[i] A.S. Bozek,[b] R. Bravenec,[c] B.D. Bray, J.D. Broesch,[b] N.H. Brooks,[b] K.H. Burrell,[b] J. Callen,[j] R.W. Callis,[b] C.S. Campo,[b] T.N. Carlstrom,[b] E. Carolipio,[k] B. Carreras,[d] W.P. Cary,[b] T.A. Casper, V.S. Chan,[b] M. Chance,[f] L. Chen,[l] E. Chin,[b] H.K. Chiu,[b] M. Chu,[b] R.J. Colchin,[d] S. Combs,[d] J.W. Cuthbertson,[h] W. Davis,[f] J.C. De Boo,[b] J.S. deGrassie,[b] R. Deranian,[m] G. Diao,[n] J.L. Doane,[b] E.J. Doyle,[o] R. Ellis,[p] T.E. Evans,[b] M.E. Fenstermacher,[a] J.R. Ferron,[b] D. Finkenthal,[q] R. Fonck,[j] E. Fredrickson,[f] J. Freeman,[b] R.L. Freeman,[b] J. Gafert,[r] S. Galkin,[s] A. Garofalo,[g] G. Garstka,[p] G. Giruzzi,[t] P. Gohil,[b] A.A. Gootgeld,[b] F. Grantham,[b] D. Gray,[h] J.M. Greene,[b] K.L. Greene,[b] C.M. Greenfield,[b] N. Greenough,[f] R.J. Groebner,[b] S. Guenter, M.J. Hansink,[b] T.E. Harris,[b] R.W. Harvey,[u] T. Hatae,[v] C. Hegna,[j] W.W. Heidbrink,[k] D.N. Hill,[a] F.L. Hinton,[b] E.H. Hoffmann,[b] J. Hogan,[d] K.L. Holtrop,[b] R.-M. Hong,[b] W. Houlberg,[d] C.L. Hsieh,[b] D.A. Humphreys,[b] A.W. Hyatt,[b] H. Ikezi,[b] R.C. Isler,[d] G.L. Jackson,[b] N. Jaluka,[w] T.H. Jensen,[b] T. Jernigan,[d] R.D. Johnson,[b] L. Johnson,[f] D.H. Kaplan,[b] K.M. Keith,[b] A.G. Kellman,[b] D.H. Kellman,[b] R. Khayrutdinov,[x] J.F. Kinsey,[y] R.J. La Haye,[b] G. Labik,[f] L.L. Lao,[b] C.J. Lasnier,[a] E.A. Lazarus,[d] R.L. Lee,[b] J. Lee,[h] R.A. Legg,[b] R. Lehmer,[h] A.W. Leonard,[b] J.A. Leuer,[b] Y.R. Lin-Liu,[b] J.M. Lohr,[b] T.C. Luce,[b] S. Luckhardt,[h] V. Lukash,[x] J. Luo,[l] J.L. Luxon,[b] M.A. Mahdavi,[b] R. Maingi,[d] C.C. Makariou,[b] J. Mandrekas, B.B. McHarg Jr.,[b] G.E. McKee,[j] W.H. Meyer,[a] K.R. Middaugh,[b] R.L. Miller,[b] P.K. Mioduszewski,[d] J. Moller,[a] R.A. Moyer,[h] M. Murakami,[d] A. Nagy,[f] G.A. Navratil,[g] A. Nerem,[b] W. Nevins,[a] D.E. Nilson,[a] L.E. Nissley,[b] R.C. O'Neill,[b] T.H. Osborne,[b] L. Owens,[d] P.B. Parks,[b] R. Parsell,[f] A.W. Peebles,[o] B.G. Penaflor,[b] Q. Peng,[b] R. Perkins,[f] P.I. Petersen,[b] T.W. Petrie,[b] C.C. Petty,[b] J.C. Phillips,[b] D.A. Piglowski,[b] R.I. Pinsker,[b] P.A. Politzer,[b] D. Ponce,[b] G.D. Porter,[a] R. Prater,[b] S.G. Pronko,[b] A. Punjabi,[w] A. Ramsey,[f] E.E. Reis, Jr.,[b] D.E. Remsen,[b] C. Ren,[j] M.E. Rensink,[a] C.L. Rettig,[o] T.H. Rhodes,[o] B.W. Rice,[a] J.I. Robinson,[b] D. Ross,[c] C. Rost,[aa] S. Sabbagh,[g] S. Sakurai,[v] R.I. Savercool,[b] J.M. Schachter,[b] M.J. Schaffer,[b] D.P. Schissel,[b] J.T. Scoville,[b] D.L. Sevier,[b] T.C. Simonen,[b] S.M. Skinner,[b] J.P. Smith,[b] R.T. Snider,[b] H.E. St John,[b] W. Stacey,[z] G.M. Staebler,[b] B.W. Stallard,[a] R.D. Stambaugh,[b] E.J. Strait,[b] E. Synakowski,[f] P.L Taylor,[b] T.S. Taylor,[b] T. Terpstra,[f] D.M. Thomas,[b] S. Turgarinov,[x] A.D. Turnbull,[b] R. Vernon,[j] M.R. Wade,[d] M.I. Walker,[b] R.E. Waltz,[b] W.R. Wampler,[e] Z. Wang,[n] A.M. Warner,[b] J.G. Watkins,[e] W.P. West,[b] J. Whaley, Jr.,[e] D.G. Whyte,[h] H. Wilson,[bb] N. Wolf,[a] R. Wolf,[r] C.P.C. Wong,[b] K. Wong,[f] F. Yin,[l] L. Zeng,[o] M. Zerbini,[cc] C. Zhang[l]

[a] Lawrence Livermore National Laboratory, Livermore, CA.
[b] General Atomics, San Diego, CA.
[c] University of Texas at Austin, Austin, TX.
[d] Oak Ridge National Laboratory, Oak Ridge, TN.
[e] Sandia National Laboratories, Livermore, CA.
[f] Princeton Plasma Physics Laboratory, Princeton, NJ.
[g] Columbia University, New York, NY.
[h] University of California, San Diego, La Jolla, CA.
[i] Chalmers University, Götteborg, Sweden.
[j] University of Wisconsin, Madison, WI.
[k] University of California, Irvine, CA.
[l] ASIPP, Hefei, Peoples Republic of China.
[m] University of Wales.
[n] Southwest Institute, China.
[o] University of California, Los Angeles, CA.
[p] University of Maryland, College Park, MD.
[q] Palomar College, San Marcus, CA.
[r] IPP, Garching, Germany.
[s] Keldysh Institute, Moscow, Russia
[t] Assoc.-EURATOM-CEA, Cadarache, France.
[u] Comp-X, Del Mar, CA
[v] Japan Atomic Energy Research Insitute, Naka, Japan
[w] Hampton University, Hampton, VA.
[x] TRINITI, Troitsk, Russia.
[y] LeHIGH University, Bethlehem, PA
[z] Georgia Tech, Atlanta, GA
[aa] MIT, Cambridge, MA.
[bb] Culham, Abingdon, UK.
cc) ANEA, Frascati, Italy.